Dynamics of two coupled van der Pol oscillators

Ignacio Pastor-Díaz* and Antonio López-Fraguas†
Asociación EURATOM/CIEMAT para Fusión, Avenida Complutense 22, 28040 Madrid, Spain
(Received 10 June 1994; revised manuscript received 7 February 1995)

A system of two coupled van der Pol oscillators showing multistable behavior for some control parameter ranges is studied. When several attractors coexist a rich fractal structure is found both on the border between basins and in extended zones of the phase space. In such zones strong mixing and self-similar structure of basins are manifest. A relationship is observed between the appearance of symmetric attractors and the fractal properties of the attraction basins. First return maps, Poincaré sections, and probability distribution functions have been computed for the model equations, indicating that the complex dynamics found in the system can be understood in terms of more simple discrete transformations related to the logistic map. A combined master-slave system based on the coupled oscillators studied is found to enter a chaotic synchronization regime for some values of the control parameters. The practical implications of the observed phenomena are discussed.

PACS number(s): 05.45.+b, 42.65.Vh

I. INTRODUCTION

The study of systems of coupled nonlinear oscillators is significant in a number of areas of fundamental and applied mathematics and physics, such as bifurcations in the presence of symmetries [1–4], chaos theory [5–9], multistability and hysteretic behavior [10–22,24–28], nonlinear electronics, etc.

The essential elements are either self-sustained or forced pulsating elements and a sufficiently strong coupling between them, allowing for rather complex temporal behaviors that capture some of the characteristics of irregular natural phenomena.

These systems with just two or a few nonlinear coupled elements range between the relatively simple behavior of a single nonlinear oscillator (where geometric theory and the perturbative methods are highly developed) and the tremendously complex spatiotemporally extended systems such as fluids, where problems like turbulence and the dynamical generation of patterns and defects are the object of intense study today [23]. Incidentally, it is to be noted that some of these issues are dealt with using models involving a rather large number of nonlinear coupled oscillators; thus, the analysis of simpler cases can form the building blocks needed to gain insight into more complicated systems.

The model studied in this paper is given by Eqs. (1):

$$\begin{aligned} \dot{x} &= y \ , \\ \dot{y} &= (\varepsilon_1 - (x+\beta z)^2) y - (x+\beta z) \ , \\ \dot{z} &= v \ , \\ \dot{v} &= (\varepsilon_2 - (z+\alpha x)^2) v - (z+\alpha x) \ , \end{aligned} \tag{1}$$

which were considered in some detail in [4]. In that reference it was found that chaotic behavior is possible for (1), the role of the discrete symmetries of the vector field in the dynamics was discussed, and multistability was reported.

The physical meaning of Eqs. (1) is that of two van der Pol oscillators coupled by adding to each one's amplitude a perturbation proportional to the other one. For $\alpha=\beta=0$, (1) uncouples to yield two van der Pol oscillators whose limit cycles are determined (in fundamental period and amplitude) by ε_1 and ε_2.

Although the van der Pol oscillator model has been used to study a wide range of self-oscillating phenomena ranging from physics to biology, a concrete example is found in an electronic circuit with an active element (triode or transistor) in which a dynamical equilibrium is attained between amplification for low voltages and dissipation for larger ones. In this context all the conclusions drawn from the paper can be applied to a feasible and highly intuitive experimental system.

Our goal in this paper is to complete the study of the dynamical aspects of Eqs. (1), which were initiated in [4]. The additional aspects that have been addressed can be divided in two main groups: (i) the structure of attraction basins in phase space as a control parameter is varied, and its relation to the number and symmetry of the underlying attractors, and (ii) the computation of first-return maps, Poincaré sections, and probability distribution functions.

The main results obtained are the relationship between the fractal properties of attraction basins and the symmetry of the underlying attractors, and that the complex behavior found can, in all the cases studied, be approximated quite well by simple discrete transformations similar to the logistic map.

Finally, the system can be configured in a master-slave setup given by

$$\left.\begin{aligned} \dot{x} &= y \ , \\ \dot{y} &= (\varepsilon_1 - (x+\beta z)^2) y - (x+\beta z) \ , \\ \dot{z} &= v \ , \\ \dot{v} &= (\varepsilon_2 - (z+\alpha x)^2 - (z+\alpha x) \ , \end{aligned}\right\} \text{(master)}$$

*Electronic address: pastor@craya.ciemat.es
†Electronic address: fraguas@craya.ciemat.es

$$\left.\begin{aligned}
&\dot{x}_1 = y_1 \ , \\
&\dot{y}_1 = (\bar{\varepsilon}_1 - (x + \bar{\beta} z_1)^2) y_1 - (x + \bar{\beta} z_1) \ , \\
&\dot{z}_1 = v_1 \ , \\
&\dot{v}_1 = (\bar{\varepsilon}_2 - (z_1 + \bar{\alpha} x)^2 - (z_1 + \bar{\alpha} x) \ ,
\end{aligned}\right\} \text{(slave)}$$

that shows chaotic synchronization for some combinations of the control parameters. The main reason for studying a master-slave system like (2) is that we thought it would be interesting to check the possibility that the system of two coupled van der Pol oscillators considered as a whole could act on a similar one (slave system) giving rise to chaotic synchronization. This phenomenon, reported originally in [29] and developed further in [30–34], has straightforward technological applications in data encoding, for example.

The rest of the paper is organized as follows: in Sec. II we present the numerical techniques used to study Eqs. (1) and (2), together with the bulk of the results, and in Sec. III the conclusions and perspectives for future work are outlined.

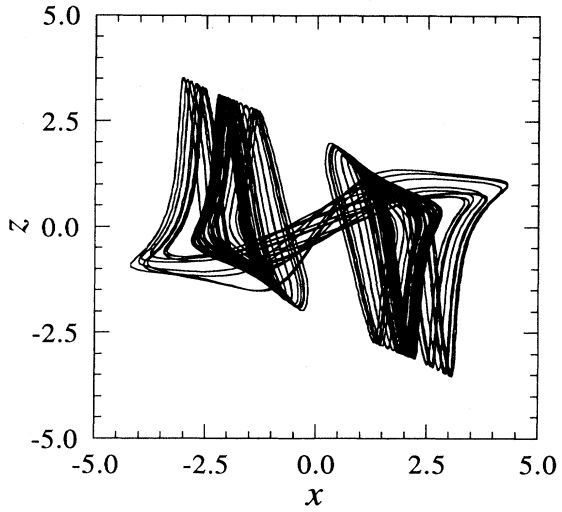

FIG. 1. Three chaotic attractors coexist for Case A, $\alpha = 0.5$; one of them is symmetric, the other two are asymmetric with respect to an inversion through the origin.

II. NUMERICAL METHODS AND RESULTS

A. Numerical methods

The main tool used in this investigation was a fourth-order Runge-Kutta (RK) algorithm allowing the numerical integration of model equations (1) and (2). The implementation of the method was different, however, when used to study the basins' fractal structure or the first-return maps, Poincaré sections, and probability distribution functions. For the basins' structure computations a vectorized fourth-order RK algorithm was written as part of the main program.

When two or more attractors are found simultaneously (see Fig. 1), a criterion is needed to classify a given phase space point as pertaining to one of the attraction basins. This is done in our case by computing the long-term average of a system variable (x or z, say) or a power of it. That quantity turns out to be different enough for different attractors to allow the classification of all phase space points studied. Of course, this criterion does not reveal whether the underlying attractor is chaotic or regular (limit cycle), but one of the results we obtain is that the attraction basin structure is, in a broad sense, not very sensitive to that feature but, rather, to the number and symmetry of the attractors.

It must be pointed out that a classifying criterion that is always valid for all the parameter combinations explored is not known *a priori,* partly due to the fact that attractors can be created or destroyed as a parameter is varied. In this sense the criterion used to classify phase space points must be tailored to each of the explored cases.

Only a two-dimensional section of the total four-dimensional phase space of (1) is amenable to a detailed computation, even using a rather powerful computer. Initial conditions of the form $(x,0,z,0)$ have been investigated with both x and z taking values on the interval $[-5.0,5.0]$ (or a subset of it). Arrays of 256×256 or 512×512 initial conditions have been integrated. Symmetry considerations allow the actual number of computations to be reduced by one half in some instances, because the attraction basin to which a point $(-|x|,0,-|z|,0)$ pertains is completely determined by the one at $(|x|,0,|z|,0)$.

For the rest of the computations mentioned above, standard NAG library routines have been used. The techniques for obtaining first-return maps and Poincaré sections from autonomous systems are well known and a good description of them can be found in [35].

The probability distribution functions for variables x and z were obtained by dividing their range into a sufficiently high number of bins (1000) and counting the number of times that the signal passes through each one of them in a very long, small step size integration.

B. Attraction basins' structure

The computations made to clarify the attraction basins' structure for Eqs. (1) concentrate mainly on two combinations of control parameters, which have been named Case A and Case B. Case A corresponds to $\varepsilon_1 = \varepsilon_2 = 1.0$, $\beta = -1.75$, with α varying in the interval [0.2,0.7], while Case B corresponds to $\varepsilon_1 = 1.0$, $\varepsilon_2 = 2.0$, $\beta = -0.75$, and α in the interval [0.9600,1.0955]. Inside this interval two ranges are to be distinguished: for α in [0.96,0.98] only one fully symmetric chaotic attractor is found, while for slightly higher values of the control parameter a symmetry-breaking bifurcation takes place. Several attractors coexist in both Case A and Case B, giving rise to a nontrivial structure of the corresponding attraction basins. The main difference is that while in Case A symmetric and asymmetric attractors coexist for some range of the control parameter α, in Case B only asymmetric attractors are found for $\alpha > 0.98$. Another difference worth mentioning is that in Case A all the at-

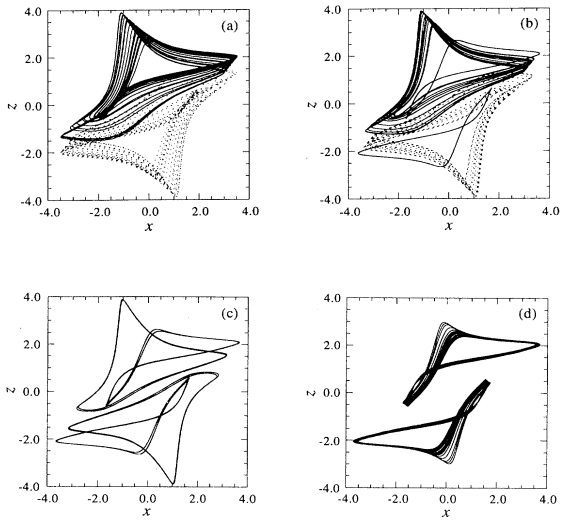

FIG. 2. An x-z projection of the main dynamical features of Case B with α varying in [0.9900,1.0955]. (a) Two chaotic asymmetric attractors coming from a symmetry-breaking bifurcation ($\alpha=0.99$); (b) two new asymmetric limit cycles along with the old chaotic attractors ($\alpha=1.055$); (c) an inverse cascade leads to asymmetric periodic attractors, while the limit cycles born at $\alpha=1.055$ double their period ($\alpha=1.0405$); and (d) only two chaotic attractors remain, coming from the solutions born at (b) ($\alpha=1.0955$).

tractors found are chaotic, while in Case B we begin with two asymmetric chaotic attractors (coming from the symmetry-breaking bifurcation), then two asymmetric limit cycles appear (for $\alpha\approx 1.0055$), and for higher values of α both the chaotic and limit cycle attractors suffer a series of bifurcations. At $\alpha\approx 1.025$ the formerly chaotic attractors become periodic (through an inverse cascade) and at $\alpha\approx 1.0405$ the limit cycles that appeared previously double the period. At a value of $\alpha\approx 1.0955$ the two periodic attractors disappear, and what remains are two other chaotic attractors coming from the solutions born at $\alpha\approx 1.0055$ (Figs. 2 and 3).

The two cases mentioned above have been selected mainly because previous experience was gathered about them ([4]) and also because they are representative in the sense that they show two of the most complex behaviors found for system (1), at least from the point of view of the number of coexisting attractors (a maximum of 3 for Case A and 4 for Case B). Although several tens of combinations of control parameters have been explored, no more than four coexisting attractors in phase space have ever been found, but nevertheless the possibility of an even greater number is not ruled out.

Let us begin with the discussion of Case A. For α values in the intervals [0.20,0.48] and [0.52,0.70] two asymmetric chaotic attractors are found, while for α in [0.483,0.510] another symmetric chaotic attractor is added (see Fig. 1). For α values near the symmetric attractor creation or destruction, the basin structure consists of zones where both basins are clearly separated and others where an intense mixing of basins and self-similarity at smaller scales takes place (Fig. 4). Successive blowups of a mixed area for other values of α reveal that self-similar structure and strongly fractal boundaries are also observed (Fig. 5). On each scale solid (open) bands pertaining to each basin are intermingled with zones in which an apparently uniform mixing of both basins takes place. On further magnification such zones reveal similar structures, giving evidence of a fractal, Cantor-like structure of the basins.

A quantitative characterization of the fractal structure of basins is given through the uncertainty exponent, computed following [11]. This exponent has been calculated for $\alpha=0.2$, 0.3, 0.4, 0.5, 0.6, and 0.7. Good power scaling of the uncertain fraction with size is obtained in all the cases [Fig. 6(a)]. The uncertainty exponent is significantly lower outside the bifurcation value ($\alpha\approx 0.5$) than for $\alpha=0.5$, where a symmetric attractor is also found [Fig. 6(b)].

On the basin boundary, smooth segments alternate with fractal regions. A similar behavior displaying fractal boundary basins has been found in systems having more than one attractor [10–18]. A related but different basin structure is found in the so called riddled basins [19–21], in which any neighborhood of every point in the riddled basin has points belonging to the other. In spite of the differences, in both kinds of basin structures one is very likely to find strong final state sensitivity with respect to small changes to the initial conditions. From this point of view a precise knowledge of the position and extent of such zones may prove of interest in the design of systems exhibiting at least safe qualitative dynamics (i.e., qualitative dynamics that does not change under a

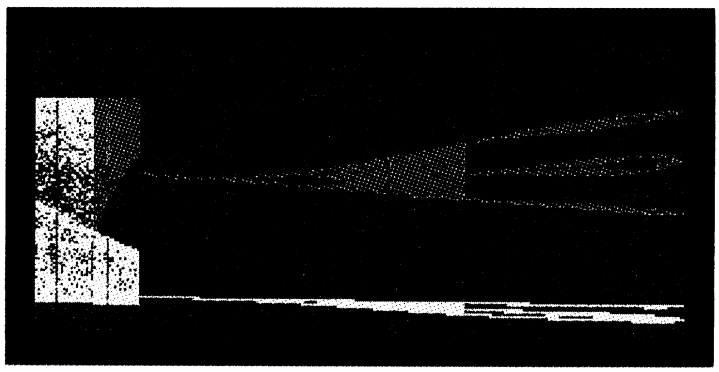

FIG. 3. Bifurcation diagram for Case B. On the abscissas the control parameter α ranges between 0.96 and 1.20 and on the ordinates the z variable relative maxima are shown. The different colors correspond to four different initial conditions that are followed through the whole α range. The existence of several attractors for some values of the control parameter as well as their bifurcations are apparent.

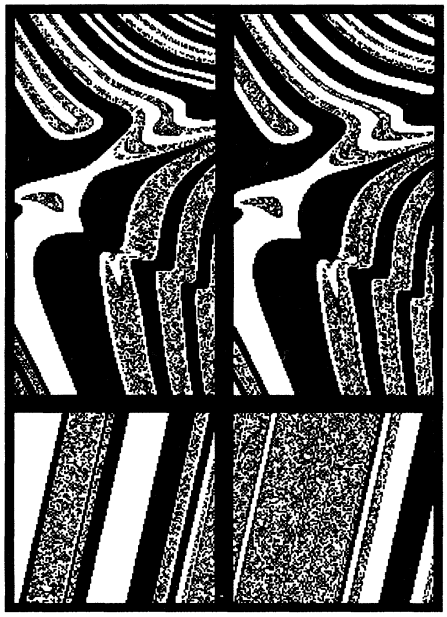

FIG. 4. Attraction basin structure of Case A just before ($\alpha=0.48$, top left) and after ($\alpha=0.52$, top right) the creation (destruction) of the symmetric attractor. Initial conditions $(x,0,z,0)$ are plotted, with x in [0.0,5.0], z in $[-5.0,5.0]$. Black represents points in phase space going to the attractor with $\langle x \rangle > 0$ and white represents points going to the attractor with $\langle x \rangle < 0$. Strong mixing among black and white zones is observed over extended areas of phase space and is found at smaller scales (self-similarity) as shown in the blowups of the bottom panels, corresponding to $\alpha=0.48$. Bottom left panel $x \in [3.298,3.302]$ and $z \in [-0.402,-0.398]$; bottom right panel $x \in [3.2991,3.2995]$ and $z \in [-0.4000,-0.3996]$.

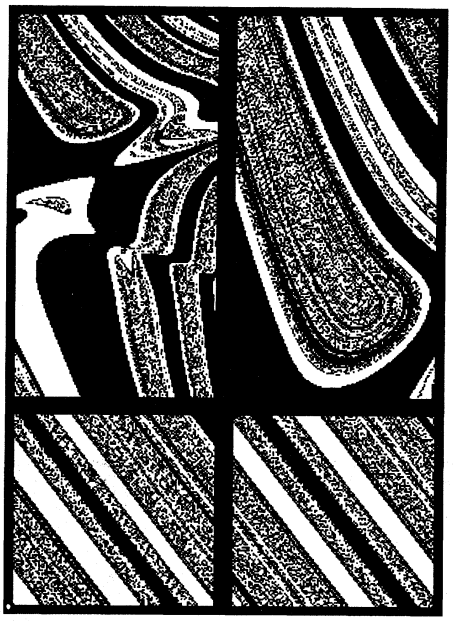

FIG. 5. Attraction basin structure blowups (Case A, $\alpha=0.35$) showing that the mixed zones manifest a self-similar, fractal structure. From top to bottom and from left to right, $x \in [0.0,5.0]$, $z \in [-5.0,5.0]$; $x \in [0.0,3.2]$, $z \in [1.7,5.0]$; $x \in [1.0,1.1]$, $z \in [3.56,3.6]$; $x \in [1.072,1.082]$, $z \in [3.611,3.621]$.

small modification of initial conditions).

When the symmetric attractor appears, its attraction basin rather suddenly takes over most of the mixed zones that existed previously. In this sense basin structure changes sharply at the bifurcation value, as shown by the uncertainty exponent [Fig. 6(b)]. While the symmetric attractor exists, attraction basins are quite regularly distributed over phase space except for very delicate and thin fractal structures on the border between them (Fig. 7). As the symmetric attractor disappears, it leaves behind zones of intense basin mixing where previously its own attraction basin was located (see Fig. 4).

In Case B and for α in [0.9905,1.0005] the attraction basins of the two coexisting attractors (asymmetric and chaotic) are regularly and smoothly distributed in phase space as alternating bands of different thickness. Small structures are apparent as very thin interrupted curves near the boundary between them, no evidence of extended zones with strong basin mixing is found, which distinguishes this case from Case A.

For $\alpha \approx 1.005$, two new asymmetric limit cycles appear and their attraction basins grow steadily as α increases. Near the bifurcation point, they show as thin structures sometimes located near the boundary of the previous ones. When $\alpha=1.0955$ the solutions born at $\alpha \approx 1.005$

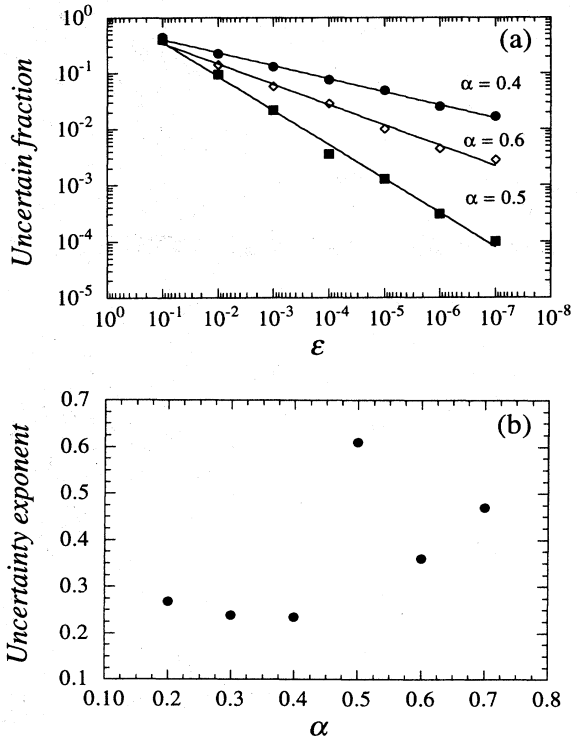

FIG. 6. (a) Scaling of the uncertain fraction with size for $\alpha=0.4$, 0.5, 0.6 (Case A), and (b) uncertainty exponent as a function of the control parameter. Note the increase (decrease) of this exponent at α values around the bifurcation that creates (destroys) the symmetric attractor.

are the only ones that survive. In this situation, the global structure of their attraction basins is (but for minor details) identical to the original one (Fig. 8). The overall process can be interpreted as an exchange of basins from the previous chaotic attractors to the ones remaining at $\alpha=1.0955$. The exchange occurs in a way that points in phase space that went to the chaotic attractor with $\langle z\rangle<0$ ($\langle z\rangle>0$) now go to the attractor with $\langle z\rangle<0$ ($\langle z\rangle>0$), although the asymptotic dynamics is completely different from the chaotic attractor. In that sense the basin structure seems to be much more robust than asymptotic behavior, at least for small changes in a control parameter. Even when four asymmetric attractors coexist, no zone in phase space with an extended basin mixing as in Case *A* has been found.

The previous results lead us to propose the following conjecture: when asymmetric attractors exist, a symmetric one can appear only if an extended zone of strong basin mixing is found. It will be precisely that zone that builds the attraction basin of the symmetric attractor.

In order to give further numerical support to that conjecture, another control parameter combination that shows the same number (and kind of symmetry) of attractors than Case *A* has been studied, namely $\varepsilon_1=\varepsilon_2=1.0$, $\beta=-2.0$, α in [0.50,0.72]. Behavior similar to the one previously described is obtained, giving it partial support. It proved to be rather difficult to find the same number of attractors and symmetries if the parameters were varied a

FIG. 7. Attraction basis structure in Case *A*, $\alpha=0.50$ (top panel) and in Case *B*, $\alpha=1.0855$ (bottom panel). In the first case, three chaotic attractors coexist and the corresponding initial conditions are shown in blue (asymmetric attractor, $\langle x\rangle>0$), red (asymmetric attractor, $\langle x\rangle<0$), and green (symmetric attractor). In the second case two chaotic attractors and two limit cycles (all of them asymmetric) are found together. The coloring of the initial conditions is blue (chaotic, $\langle z\rangle>0$), red (chaotic, $\langle z\rangle<0$), green (limit cycle, $\langle z\rangle>0$) and yellow (limit cycle, $\langle z\rangle<0$). In both panels, x and z range between -5.0 and 5.0.

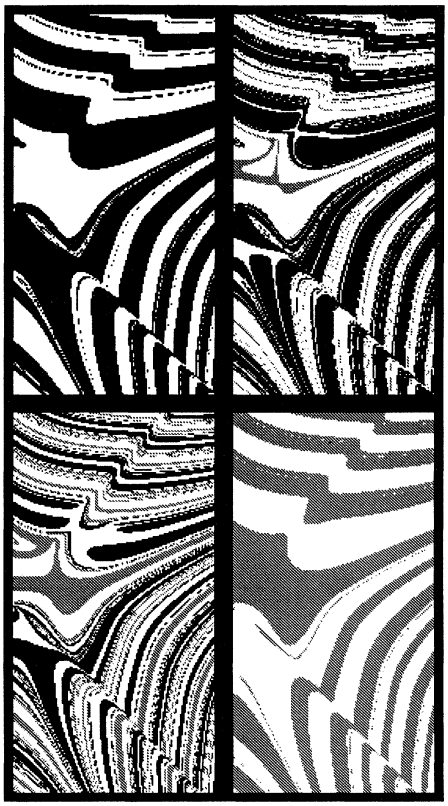

FIG. 8. Attraction basin structure and its evolution under a change in control parameter α in Case B. Top left panel $\alpha=0.9905$, top right $\alpha=1.0055$, bottom left $\alpha=1.0655$, and bottom right $\alpha=1.0955$. Black and white points represent initial conditions that go to the (initially) asymmetric chaotic attractor with $\langle z\rangle>0$ ($\langle z\rangle<0$), while dark and light gray represent conditions that go to the (initially) limit cycle with $\langle z\rangle>0$ ($\langle z\rangle<0$). In all the panels $x\in[0.0,5.0]$, $z\in[-5.0,5.0]$.

lot from the values corresponding to Case A. In such cases a different number of attractors and their symmetries is obtained, making the comparison nearly impossible.

C. First return maps, Poincaré sections, and probability distribution functions

It is known that the dynamics of many systems evolving in a continuous way in time can be considerably simplified when viewed as a discrete map obtained from the Poincaré surface of section or some of its variants, as first-return maps. The first-return map consists essentially of a plot of the $(n+1)$th relative maximum as a function of the nth maximum for a signal in which transients have decayed. If the graph of such a function lies on a curve (with a single maximum, say), then a straightforward connection with the well developed theory of unidimensional maps can be made, allowing a simplification of the overall dynamic picture.

Poincaré sections and first-return maps have been computed for model equations (1) in Case A and Case B. The dynamics can be understood in terms of much simpler discrete transformations similar to the logistic map. Let us discuss these points in more detail beginning with Case A.

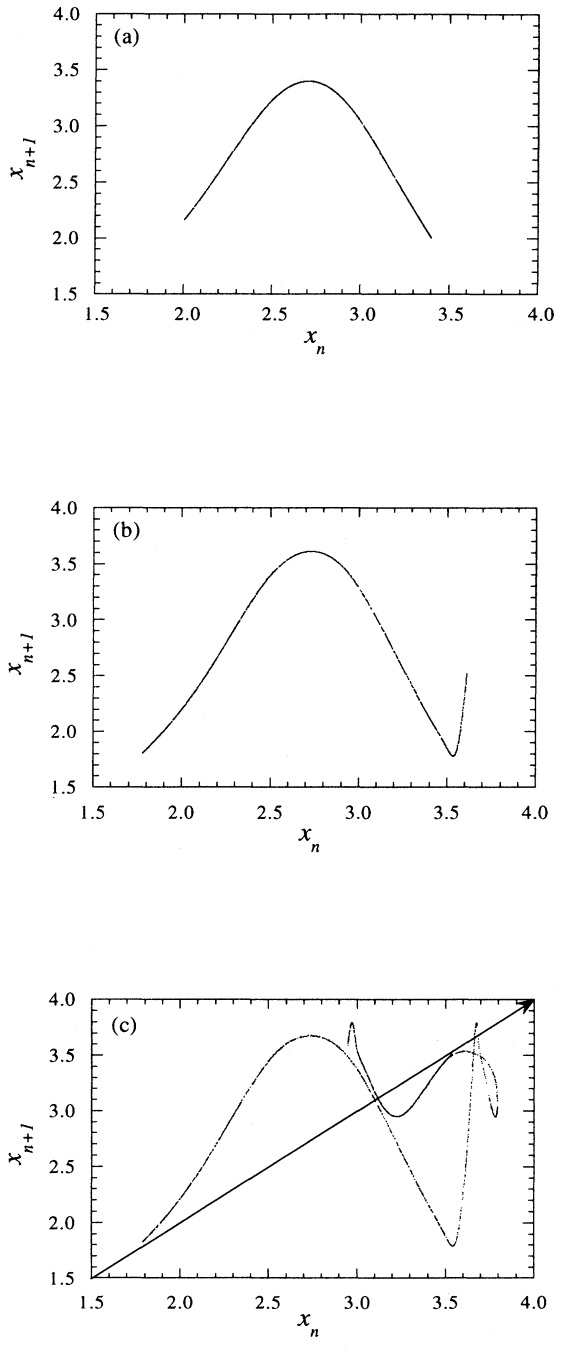

FIG. 9. First-return maps for Case B at three different values of the control parameter α. (a) $\alpha=1.00$ (asymmetric attractor); (b) $\alpha=0.985$ (asymmetric attractor); (c) $\alpha=0.98$ (symmetric attractor). Note that in (c) a tangency point with the line $x_{n+1}=x_n$ occurs, as well as a tangency among two branches of the first-return map when α takes a value very close to the symmetry-breaking bifurcation.

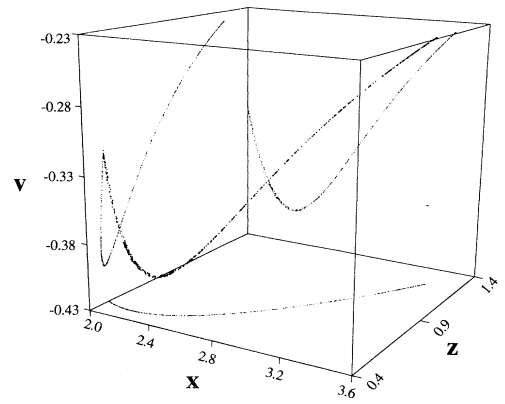

FIG. 10. Three-dimensional Poincaré map through the hyperplane $y=0$ $(dy/dt<0)$ for Case B, $\alpha=1.0$. Two-dimensional projections on the three coordinates planes are also shown.

For $\alpha=0.50$ the first-return map is quite simple for the asymmetric attractor and more complicated for the symmetric one, but in both cases the points are not scattered through the plane, but located on quite definite curves. A Poincaré section through the hyperplane $v=0$ $(dv/dt<0)$ for these attractors shows an even simpler picture: the points obtained by successively piercing the section are located on smooth curves (in $\mathbb{R}^3$), indicating that the main dynamical features can be modeled as the restriction of the Poincaré map to such invariant curves. These facts hold true over the whole explored control parameter range.

In Case B interest was focused on the transition with spontaneous symmetry breaking that takes place for $\alpha=\alpha_{sb}\approx 0.98$. If $\alpha<\alpha_{sb}$, only one chaotic, fully symmetric attractor is found, which splits into two asymmetric attractors for $\alpha\geq 0.98$. At $\alpha=1.00$ the first-return map has a smooth paraboliclike form, indicating that a direct application of the results for the logistic map to that case is straightforward [Fig. 9(a)]. When decreasing the control parameter towards α_{sb}, the first-return map develops additional structure until for $\alpha=\alpha_{sb}$ it shows a tangency point with the $x_{n+1}=x_n$ line and also a tangency point between two branches of the first-return map also located on such a line [Figs. 9(b) and 9(c)].

The Poincaré section through the hyperplane $y=0$ consists also of smooth invariant curves in $\mathbb{R}^3$. The same remarks made before can be applied here (Fig. 10).

To summarize, in all the cases where the Poincaré map has been computed, an extremely simple picture of the dynamics is apparent. The map leaves invariant one or more curves on $\mathbb{R}^3$ (corresponding to one or more asymptotic attractors), meaning that the main dynamic features of Eqs. (1) can be understood through the restriction to such invariant curves of a mapping of $\mathbb{R}^3$ in itself.

Probability distribution functions (PDFs) for the dynamical variables x and z have been computed, showing a markedly non-Gaussian behavior (see Fig. 11), which have also been reported for other kinds of nonlinear oscillators [36]. PDFs inherit the symmetry properties of the attractor for which they are computed and, in general, present rather conspicuous spikes reminiscent of the periodic solutions that generated the chaotic attractors through period doubling. In some cases, changes in the metric or topological properties of the underlying attractors can be inferred from changes in the statistical properties of PDFs (mean value, skewness, kurtosis, etc.), which makes them a valuable tool in nonlinear system diagnosis (Fig. 12).

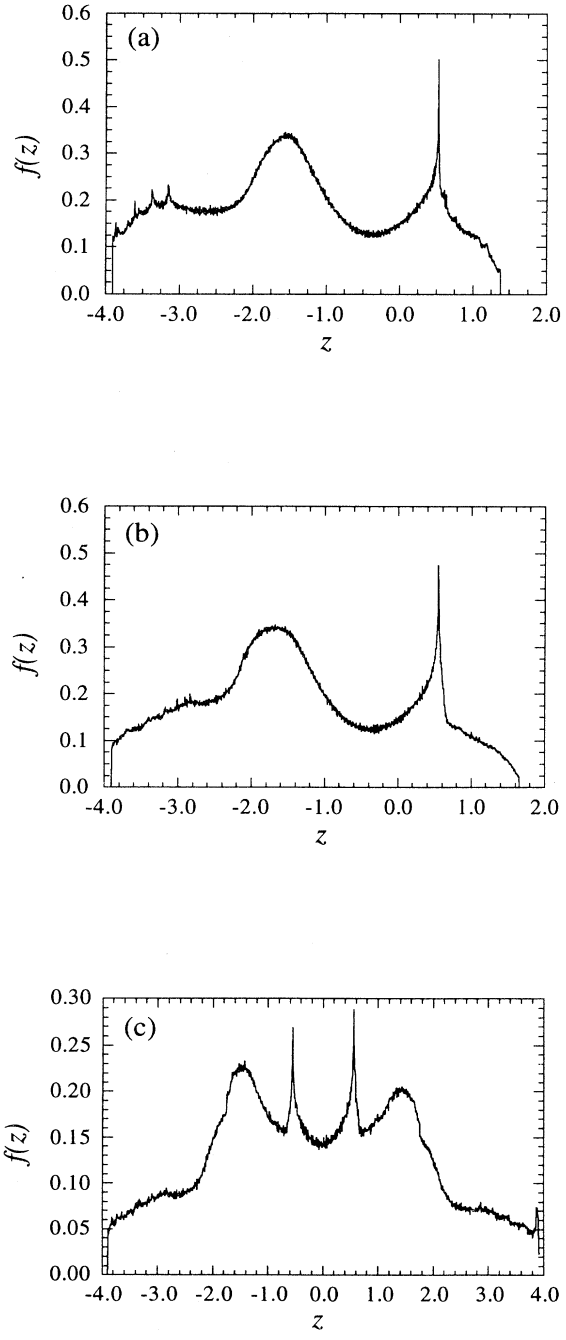

FIG. 11. z variable probability distribution function in Case B, (a) $\alpha=1.00$, (b) $\alpha=0.985$, and (c) $\alpha=0.98$.

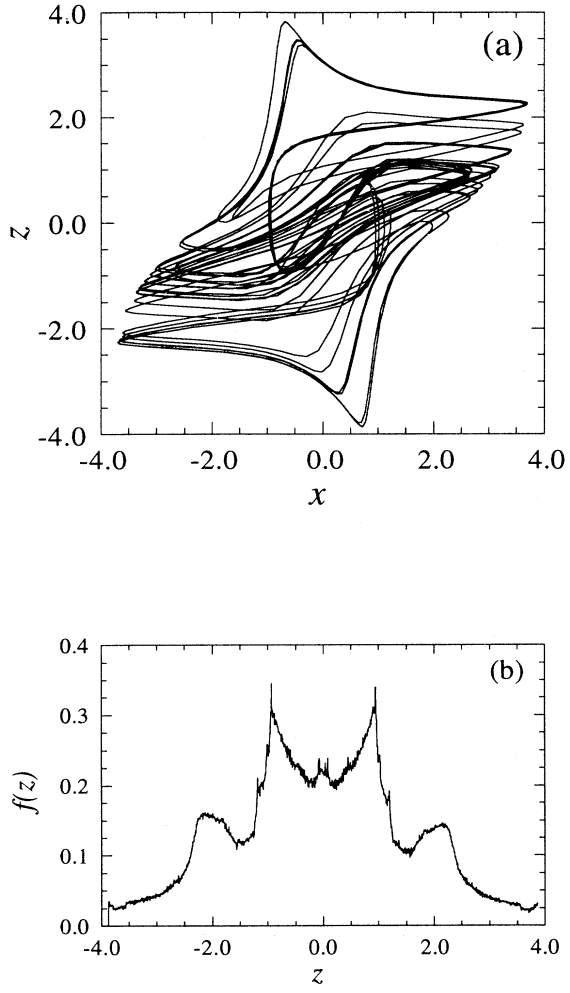

FIG. 12. (a) Symmetric chaotic attractor and (b) probability distribution function for Case B, $\alpha=1.503$. This attractor shows some geometrical differences with respect to the one at $\alpha=0.98$. These differences are enhanced in the probability distribution function, which is markedly different from the one in Fig. 11(c) in some of its statistical properties.

D. Chaotic synchronization

Equations (2) form a system consisting of a master system (1) forcing a copy of itself through the $x(t)$ variable (master-slave configuration). Chaotic synchronization has been observed for control parameters as in Case B (Fig. 13), while no synchronization is seen in Case A. The chaotic synchronization consists of two chaotic signals coming from the master and slave system keeping pace [in more formal terms $x_{\text{master}}(t)=x_{\text{slave}}(t)+b$ with b a constant that depends on the difference between the initial conditions for master and slave systems] even if they begin with rather different initial conditions. The fact that the master and slave signals differ by a constant (b) that is dependent on the difference of initial conditions for both subsystems is a feature that, to our knowledge, has not been described previously in the literature of synchronized chaos. We must point out that up to now we have not had an explanation for the role played by the initial conditions in the constant b or in general in chaotic entrainment.

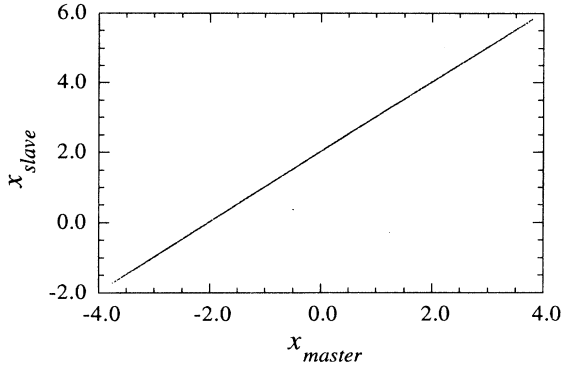

FIG. 13. An example of the chaotic synchronization phenomenon observed for Case B with control parameters in both the master and slave subsystems equal ($\alpha=0.98$). The initial conditions for master and slave differ by 0.1 in each of the variables. The mean value of the slave signal depends on the difference in initial conditions.

III. CONCLUSIONS AND PERSPECTIVES

An autonomous system of equations displaying a rich dynamical behavior has been studied.

Attraction basins have been computed for (1) and their organization in phase space has been correlated with the symmetry of the underlying attractors. At bifurcations in which new attractors appear and coexist with other ones, the overall structure of the attraction basin differs depending on the symmetry of the new attractor. When a symmetric one is born, its attraction basin basically spreads over zones that previously displayed an intense mixing between the preexisting attraction basins, and the uncertainty exponent rises significantly. Analogous behavior is found when it disappears; extended regions of its basin end up in an extreme intertwining of the surviving basins and the uncertainty exponent drops. When symmetric and asymmetric attractors coexist, the basin boundaries are more regular than when no symmetric attractor is found, but sizable fractal segments are still present.

In Case B, attraction basin evolution is clearly less abrupt, and this is correlated with the fact that no symmetric attractors are found for $\alpha>\alpha_{sb}$. The basins of the new asymmetric limit cycles spread out over the basins belonging to the previous attractor with the same $\langle z \rangle$ value. Loosely speaking, we could say that the new attractors gradually absorb more and more space in the basin of the old ones, until the latter eventually disappear.

In general, attraction basin structure is more sensitive to the number and symmetry of the underlying attractors than to their dynamical character (chaotic or regular). To our knowledge, this is one of the first instances in which such a study of attraction basin structure and its relation to the model symmetries is done for autonomous

differential equations.

It seems appropriate to offer some further comments on the roles played by symmetry and coexistence of attractors in the fractal structure of attraction basins. In our model the discrete symmetries of the vector field are an exact property of it, and this holds true when there is only one attractor, or when several coexist. Due to the particular form of the symmetry, however, when an asymmetric attractor is found, we are certain that another companion attractor exits simultaneously. Provided that more than one attractor is found, there are good chances to have attraction basins with rich fractal structure, as found in many other nonlinear systems. So the point is that although symmetry by itself doesn't imply directly multiple fractal basins, provided that the symmetry is (spontaneously) broken, the appearance of such basins with fine fractal structure is quite probable. We have never found (up to now) in our model several coexisting completely symmetric attractors. Then, the rich fractal structure of basins is tied to the existence of asymmetric attractors, and thus to symmetry breaking of at least some asymptotic solutions (attractors). Finally, the attraction basins have the same kind of symmetry of the corresponding attractor, i.e., they can be divided into symmetric basins with respect to an inversion through the origin, or appear in pairs related by that symmetry.

First-return maps and three-dimensional Poincaré sections show that the complex temporal behavior in Eqs. (1) is quite well modeled by simple discrete transformations; this result holds for both symmetric and asymmetric chaotic attractors. The Poincaré section of Eqs. (1) reduces the dynamics to a discrete map from $\mathbb{R}^3$ to $\mathbb{R}^3$ that leaves invariant a few curves (or segments of curves) on which the dynamics is essentially that of the logistic map.

Probability distribution functions have been computed systematically for Eqs. (1) providing evidence of a markedly non-Gaussian behavior, a fact observed in other nonlinear circuits and systems. In addition to this, PDFs are useful as a tool to diagnose changes in the topological or geometrical properties of attractors through the corresponding changes in some of their statistical characteristics. In that sense, PDFs should become a standard test in nonlinear systems analysis.

The results obtained in this investigation may serve to motivate further research; in particular, the authors plan to extend its work to cover some of the issues given below.

A possible way to study attraction basin organization in a (relatively) high-dimensional system akin to (1) is given by the fact that a Poincaré section of Eqs. (1) reduces the dynamics to a discrete map from $\mathbb{R}^3$ to $\mathbb{R}^3$ that leaves invariant some curves (or segments of curves). Then, if a model transformation from $\mathbb{R}^3$ to $\mathbb{R}^3$ could be devised keeping these essential features in focus, the iteration of such an application could provide valuable information on the organization of attraction basins for systems closely related to (1).

In a previous paper ([4]) it was shown that for certain ranges of the control parameter values, unbounded solutions of (1) exist. That implies the need to consider, in general, another attractor at ∞ and the shape of the corresponding attraction basin. Recent work on safe engineering design and on the so called riddled basins makes such a study also relevant for the proposed model.

A deeper investigation of the parameter space regions where the chaotic synchronization phenomenon takes place is planned, with special attention to the possibility of synchronizing several chaotic solutions when they coexist and to the observed feature that the mean value of the slave variable is a function of the distance between initial conditions for the master and slave subsystems. The practical implication of such a study will be the possibility of coding a rather large amount of information by using just one basic chaotic system and adjusting some of its control parameters and/or the initial conditions.

The relationship between the overall structure of the stable and unstable manifolds of the (in general unique) equilibrium point and the attraction basin structure is another theme for future investigations.

[1] J. J. Collins and I. N. Stewart, J. Math. Biol. **30**, 827 (1992).
[2] J. J. Collins and I. N. Stewart, J. Nonlinear Sci. **3**, 349 (1993).
[3] J. J. Collins and I. N. Stewart, Biol. Cybern. **68**, 287 (1993).
[4] I. Pastor, Víctor M. Pérez-García, F. Encinas-Sanz, and J. M. Guerra, Phys. Rev. E **48**, 171 (1993).
[5] Ulrich Parlitz and Werner Lauterborn, Phys. Rev. A **36**, 1428 (1987).
[6] V. Englisch and W. Lauterborn, Phys. Rev. A **44**, 916 (1991).
[7] M. Poliashenko, S. R. McKay, and C. W. Smith, Phys. Rev. A **44**, 3452 (1991).
[8] Maxim Poliashenko and Susan R. McKay, Phys. Rev. A **46**, 5271 (1992).
[9] D. Ruelle, *Elements of Differentiable Dynamics and Bifurcation Theory* (Academic, New York, 1988).
[10] Celso Grebogi, Steven W. McDonald, Edward Ott, and James A. Yorke, Phys. Lett. **99A**, 415 (1983).
[11] Steven W. McDonald, Celso Grebogi, Edward Ott, and James A. Yorke, Physica D **17**, 125 (1985).
[12] Celso Grebogi, Edward Ott, and James A. Yorke, Phys. Rev. Lett. **56**, 1011 (1986).
[13] Celso Grebogi, Edward Ott, and James A. Yorke, Physica D **24**, 243 (1987).
[14] Celso Grebogi, Eric Kostelich, Edward Ott, and James A. Yorke, Physica D **25**, 347–360 (1987).
[15] Celso Grebogi, Edward Ott, and James A. Yorke, Science **238**, 632 (1987).
[16] Edward Ott, *Chaos in Dynamical Systems* (Cambridge University Press, Cambridge, 1993).
[17] E. Eschenazi, H. G. Solari, and R. Gilmore, Phys. Rev. A **39**, 2609 (1989).
[18] F. Palmero and F. Romero Romero, Phys. Lett. A **179**, 337 (1993).
[19] J. C. Alexander, James A. Yorke, Zhiping You, and I. Kan, Int. J. Bifurc. Chaos **2**, 795 (1992).

[20] Eric J. Kostelich, Nature **365**, 106 (1993); John C. Sommerer and Edward Ott, *ibid.* **365**, 138 (1993).
[21] Edward Ott, John C. Sommerer, James C. Alexander, Ittai Kan, and James A. Yorke, Phys. Rev. Lett. **71**, 4134 (1993).
[22] Ying-Cheng Lai and Raimond L. Winslow, Phys. Rev. Lett. **72**, 1640 (1994).
[23] M. C. Cross and P. C. Hohenberg, Rev. Mod. Phys. **65**, 851 (1993).
[24] J. M. T. Thompson, Proc. R. Soc. Lond. Ser. A **421**, 195 (1989).
[25] J. M. T. Thomson and M. S. Soliman, Proc. R. Soc. Lond. Ser. A **428**, 1 (1990).
[26] A. N. Lansbury and J. M. T. Thomson, Phys. Lett. A **150**, 355 (1990).
[27] Henry D. I. Abarbanel, Nature **364**, 672 (1993).
[28] M. J. Clifford and S. R. Bishop, Phys. Lett. A **184**, 57 (1993).
[29] Louis M. Pecora and Thomas L. Carrol, Phys. Rev. Lett. **64**, 821 (1990).
[30] Herbert G. Winful and Lutfur Rahman, Phys. Rev. Lett. **65**, 1575 (1990).
[31] Maria de Sousa Vieira, Allan J. Lichtenberg, and Michael A. Lieberman, Phys. Rev. A **46**, R7359 (1992).
[32] Rong He and P. G. Vaidya, Phys. Rev. A **46**, 7387 (1992).
[33] Kevin M. Cuomo and Alan V. Oppenheim, Phys. Rev. Lett. **71**, 65 (1993).
[34] T. C. Newell, P. M. Alsing, A. Gavrielides, and V. Kovanis, Phys. Rev. Lett. **72**, 1647 (1994).
[35] F. C. Moon (Wiley, New York, 1992).
[36] T. L. Carrol and L. M. Pecora, Phys. Rev. Lett. **70**, 576 (1993).

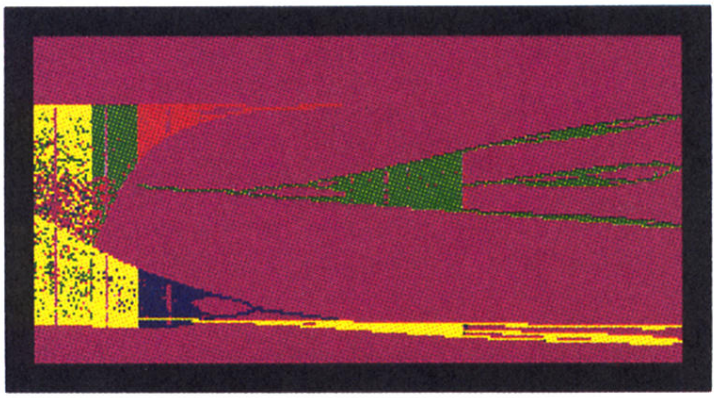

FIG. 3. Bifurcation diagram for Case *B*. On the abscissas the control parameter α ranges between 0.96 and 1.20 and on the ordinates the z variable relative maxima are shown. The different colors correspond to four different initial conditions that are followed through the whole α range. The existence of several attractors for some values of the control parameter as well as their bifurcations are apparent.

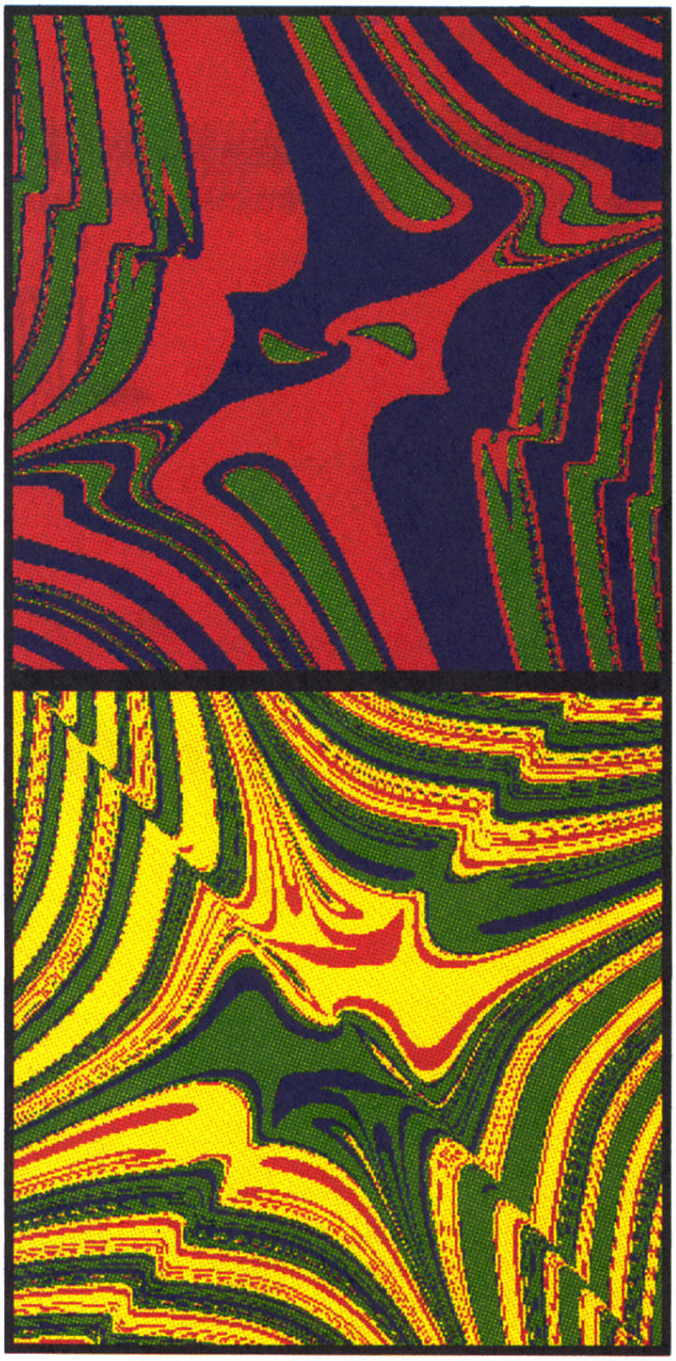

FIG. 7. Attraction basis structure in Case A, $\alpha=0.50$ (top panel) and in Case B, $\alpha=1.0855$ (bottom panel). In the first case, three chaotic attractors coexist and the corresponding initial conditions are shown in blue (asymmetric attractor, $\langle x \rangle > 0$), red (asymmetric attractor, $\langle x \rangle < 0$), and green (symmetric attractor). In the second case two chaotic attractors and two limit cycles (all of them asymmetric) are found together. The coloring of the initial conditions is blue (chaotic, $\langle z \rangle > 0$), red (chaotic, $\langle z \rangle < 0$), green (limit cycle, $\langle z \rangle > 0$) and yellow (limit cycle, $\langle z \rangle < 0$). In both panels, x and z range between -5.0 and 5.0.